Reaction Kinetics, Mechanisms and Catalysis (2024) 137:1189–1207
https://doi.org/10.1007/s11144-024-02567-4

A low cost bio-composite derived from potato plant waste (PPW-ZnO) for the removal of Rhodamine B

Khadidja Hamida[1] · Hanane Rehali[1] · Hayet Menasra[2] · Fedia Bekiri[3] · Amel Aidi[1]

Received: 5 December 2023 / Accepted: 7 January 2024 / Published online: 16 January 2024

Abstract

This work aims to synthesis activated carbon material from potato plant waste (abbreviated as PPW) and examine the material's ability to adsorb a cationic dye, namely Rhodamine B (RhB). $ZnCl_2$ was used in the chemical preparation process to produce the activated carbon composite, also known as PPW-ZnO, which was achieved by pyrolyzing the precursor for 3 h at 600 °C. Many methods, such as Brunauer–Emmett–Teller (BET), scanning electron microscopy, X-ray diffraction, Fourier transform infrared, and pH of the point of zero charge pH_{PZC}, were used to characterize the PPW-ZnO composite. The PPW-ZnO bio composite also has a porous structure, according to the study's findings, with a pore size of 6.201 nm and a specific surface area (S_{BET}) of 134.59 m^2/g. The RhB dye was adsorbed onto the PPW-ZnO bio composite, and after 120 min of agitation, the amount adsorbed reached 98.95%. The pseudo-second order model kinetic and Freundlich model isotherm were best described the adsorption process.

Keywords Adsorption · Bio-composite · Rhodamine B (RhB) · Isotherms · Kinetic

Introduction

The various forms of pollution constitute a serious risk to our environment and consequently to our health, The disposal of these items should be conducted in a manner that does not result in any detrimental effects on the environment [1–3]. The presence of dyes and pigments in water is a prominent and unwanted pollution

✉ Khadidja Hamida
Khadija.hamida@univ-biskra.dz

[1] Laboratory of LARGHYDE, University of Biskra, Bp 145 RP, 07000 Biskra, Algeria

[2] Laboratory of Applied Chemistry, University of Biskra, 07000 Biskra, Algeria

[3] Scientific and Technical Center Research On Arid Regions, University of Biskra, 07000 Biskra, Algeria

among the numerous contaminants, these dyes which are frequently synthesized, have intricate aromatic structures that give them exceptional resistance to light, heat, and oxidizing agents [4, 5]. Regrettably, their chemical durability also translates to their prolonged presence in the natural environment, resulting in limited biological degradation [6].

It is now urgently necessary to address the issue of dye and pigment pollution in water, which has led to the development of numerous treatment technologies targeted at their elimination [7, 8]. The physicochemical treatment approach of adsorption onto activated carbon has shown to be one of the most dependable and efficient among these technologies [9, 10]. The efficacy of this technology is in its capacity to extract these tenacious pollutants from water in a selective manner, hence reducing the negative consequences of dye and pigment pollution on the environment and human health [11]. In this investigation of pollution and its solutions, we examine the problems caused by artificial coloring and the critical function activated carbon plays in mitigating environmental pollution [12, 13]. Rhodamine B (RhB), a dye with basic properties, is widely recognized and utilized as a highly adaptable and essential coloring agent across multiple sectors and applications. These include dyeing fabrics such as cotton, wool, silk, nylon, paper, and leather [14, 15]. Potatoes are one of the important crops in Algeria and are widely grown in southern Algeria, especially the Oued Souf region. These many crops leave huge amounts of potato plant (stem, leaves, and roots) that are burned or used as food for animals. Reused as a raw material in the field of adsorption of pollutants from water is a strong competitor for their availability in large quantities. Because of its small porous structure its surface is changed by chemicals to increase the surface area for the adsorption process.

Several different chemical activating agents have been studied by numerous researchers in recent years to create a high surface area and a porous structure [16], including H_3PO_4 [17], H_2SO_4[18], KOH [19], and $ZnCl_2$ [20]. Zinc chloride has been extensively investigated under various preparation conditions [21–23]. This research focuses on modifying the carbon surface to significantly increase surface area and create pores, thereby enhancing the material's capacity to adsorb organic pollutants [24, 25]. In contrast, Li Y and Liu X, researchers found that employed the impregnation of $ZnCl_2$ onto the carbon matrix at a high temperature [26], creating a bio-composite based on zinc oxide [27]. This process integrates exceptional chemical and thermal stability into the activated carbon, ensuring optimal efficiency and minimizing potential adverse effects of pollutants, such as dyes [28].

The objective of this work was to remove rhodamine B (RhB) from an aqueous solution using activated carbon composite (PPW-ZnO), which was made from potato plant waste (PPW) from the Oued Souf region of Algeria by chemical activation with zinc chloride ($ZnCl_2$), a distinctive porous structure gives, surface area, extreme affinity and most important the availability of biomass is mostly free and also easy to regenerate, for RhB adsorption compared with different materials such as Graphite/CNT Composites [29], Coconut Shell Activated Carbon/$CoFe_2O_4$ Composite [30], Powdered Activated Carbon Composite [31]. This study aims to examine how well the activated carbon composite that has been created may be used to extract RhB dye from aqueous solutions. The impacts of several parameters, such as

temperature, initial concentration, ionic strength, pH of solution, and contact time, were examined. The investigation also examined adsorption kinetics, isotherms, and thermodynamic characteristics.

Materials and Methods

Preparation of PPW-ZnO bio composite

Potato plant waste (PPW) was obtained from Algeria's Oued Souf region as an absorbent. After cleaning any surface contaminants with distilled water, the PPW were dried for 24 h at 110 °C using a steel blender to grind them to a fine powder. Next, 5 g of powder was impregnated with 45 ml of $ZnCl_2$ (0.5M) and stirred for 1 h. The mixture was then dried for 7 h at 105 °C and carbonized for 3 h at 600 °C. After obtaining the activated carbon composite (PPW-ZnO), it was cleaned to remove all chloride using distilled water, brought to a neutral pH, and dried for 24 h at 105 °C [32]. The following steps in Fig. S1 illustrate the preparation of activated carbon composite PPW-ZnO.

Dye solution preparation

Rhodamine B (RhB), or CI = 45,170, is a chemical compound with the molecular formula $C_{28}H_{31}ClN_2O_3$ and a 479.02 g/mol molar mass. It is sourced from the company Biochem Chemopharma. Additionally, RhB has a maximum absorption wavelength (λ_{max}) of 554 nm. Stock dye solutions with a concentration of 500 mg/L were made by dissolving 0.5 g of dye in 1 L of distilled water [33].

Batch adsorption experiments

Adsorption studies using an adsorbent dosage of 1 g/L (PPW-ZnO) were conducted in 100 mL of RhB solution. Subsequently, a syringe filter with a pore size of 0.22 µm was employed to separate the PPW-ZnO and solution samples. A spectrophotometer called the photoLab DR 6000 UV–VIS was used to measure a residual concentration of RhB at wavelength of 554 nm. The parameter under investigation is as follows:

The following operating parameters were used to study the kinetics of RhB removal for PPW-ZnO: ambient temperature, 1 g/L of PPW-ZnO dose, and 20 mg/L of RhB concentration. Adding 1 mol/L of HCl or 1 mol/L of NaOH to the experimental solutions, pH 2–12, was tested for an equilibrium time of 120 min and a 20 mg/L beginning concentration.

Temperature effects at 20, 30, and 50 °C with initial concentrations of RhB 20 mg/L. The following formulas were used to determine the quantity of adsorbed dye per gramme of PPW-ZnO at equilibrium, or qe (mg/g), the amount of adsorption at time t, or qt (mg/g), and the removal percentage, or % removal [34, 35]:

$$\mathrm{qe} = \frac{(C_0 - C_e)V}{w}(\mathrm{mg/g}) \tag{1}$$

$$\mathrm{qt} = \frac{(C_0 - C_t)V}{w}(\mathrm{mg/g}) \tag{2}$$

$$\%\mathrm{R} = \frac{(C_0 - C_e)}{C_0} \times 100 \tag{3}$$

here C_0, C_e and Ct are the initial, equilibrium concentrations of dye and the concentration of dye solution at time t (mg/L). V is the volume of dye solution (L) and W is the weight of adsorbent used (g).

Three standard kinetic models and three adsorption isotherms were used in this work to study the adsorption mechanisms, the pseudo-firs order (PFO), pseudo-second order (PSO), Elovich, and intra-particle diffusion fractional order models are indicated as Eqs. 4, 5, 6, and 7, as shown in Table 1, Eqs. 8, 9, and 10 apply to the Langmuir, Freundlich, and Temkin isotherms. The non-linear regression analysis of the following models was examined using the capabilities available in the Origin software. Correlation (R^2) and chi-square (χ^2) values to calculate and represent the fitted model that describes the process of RhB dye adsorption onto the PPW-ZnO.

$$R^2 = 1 - \frac{\sum \left(q_{e,exp} - q_{e,cal}\right)^2}{\sum \left(q_{e,exp} - q_{e,mean}\right)^2} \tag{11}$$

$$\chi^2 = 1 - \frac{\sum \left(q_{e,exp} - q_{e,cal}\right)^2}{q_{e,cal}} \tag{12}$$

here $q_{e,mean}$ (mg/g) is the average of q_e experimental values, The best suitable equation is for the highest R^2 and the smaller χ^2 values [36].

PPW-ZnO reusability and regeneration

Reducing waste generated and operating costs are the main objectives of the laden activated carbon reusing process. For many adsorption cycles (reuse), desorption, and regeneration testing, 500 ml of RhB dye solution 20 mg/L was mixed with 0.5 g of PPW-ZnO bio composite in this investigation. When the percentage of RhB dye removal declined to less than 50%, the adsorbent was washed using a 0.1M HCl solution for 2 h. In order to employ the adsorbent in a new adsorption experiment (regeneration), it was then cleaned with distilled water and dried [43].

Table 1 Equations and parameters of the kinetic and isotherm models

	Equations	Parameters	Refs
Kinetic models			
Pseudo-first order	$q_t = q_e(1 - e^{k_1 t})$ (4)	q_e and q_t (mg/g): the adsorbed amount of RhB dye at the end and at time t,	[37]
Pseudo-second order	$q_t = \frac{q_e^2 k_2}{1+q_e.k_2.t}$ (5)	K_1 (L/min) and K_2 (g /mg min): the constants of PFO and PSO	[38]
Elovich	$q_t = \frac{1}{\beta}\ln(\alpha\beta t + 1)$ (6)	α initial adsorption rate, β desorption constant during each experiment	[39]
Intraparticle diffusion	$q_t = K_{IP} t^{(\frac{1}{2})} + C$ (7)	K_{IP} (mg/g $min^{0.5}$): the intraparticle diffusion constant	[40]
Isotherm models			
Langmuir	$q_e = \frac{Q^0_{max}.K_L.C_e}{1+K_L.C_e}$ (8)	Ce: the concentration of RhB dye at equilibrium. $Q^0{}_{max}$ (mg/g): the maximum, capacity of the monolayer, adsorption (of Langmuir)	[41]
Freundlich	$q_{e=}K_F.C_e^{1/n}$ (9)	K_L (L/mg), K_F [(mg/g)/$(mg/L)^{1/n}$]: the constant of Langmuir and Freundlich isotherm. n_F: the dimensionless, parameter of intensity (of Freundlich)	[41]
Temkin	$q_e = B\ln(K_T C_e)$ (10)	K_T (L/mg) and B: the equilibrium constants and the heat of adsorption	[42]

Results and discussion

Characteristics of PPW-ZnO

BET analysis

The surface area is one of the most crucial adsorbent qualities, Using Micromeritics ASAP 2020 Plus. The PPW-ZnO surface area was determined to be 134.59 m^2/g, as depicted by the N_2 adsorption–desorption isotherm in Fig. 1. The generated sample was 6.201 nm pore size, further demonstrated mesoporous on the surface of activated carbon.

Mesopores are present in the bio composite because, as Fig. 1 shows, the type II adsorption–desorption isotherm PPW-ZnO has a very small pore volume across the whole size distribution with H3-type hysteresis loops [44].

SEM/EDX of PPW-ZnO

SEM analysis is given in Fig. 2, utilizing the Thermoscientific Prisma E instrument. The morphology of the PPW-ZnO exhibited the presence of craters on the surface, before adsorption as a result of the activation process [45]. These craters played a role in enhancing the surface area following activation. According to this research (as shown in Fig. 2a), it is evident that the presence of zinc species during sample preparation results in "craters" with rough walls and surfaces that have varying pore sizes, diameters, and empty spaces. Fig. 2b displays the surface morphology of

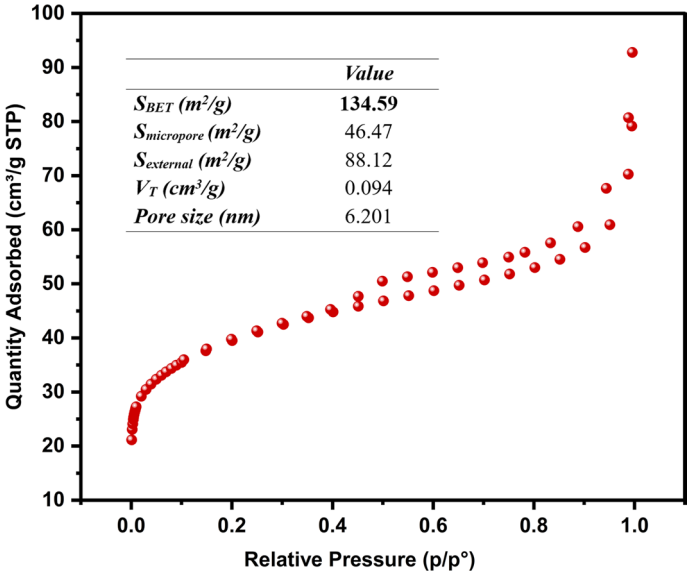

Fig. 1 The isotherm of N_2 PPW-ZnO bio composite adsorption–desorption

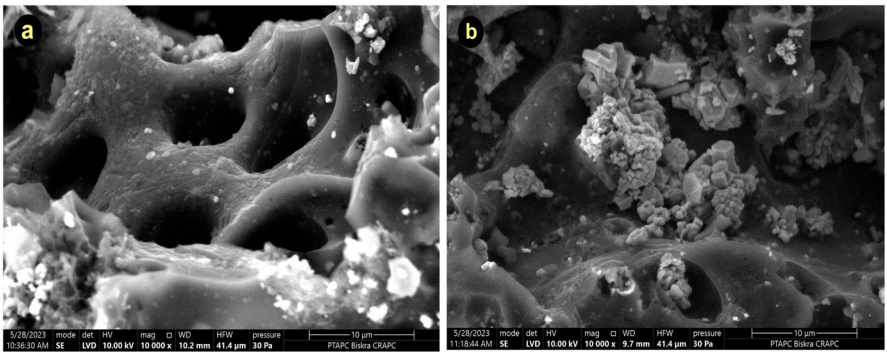

Fig. 2 SEM micrographs of PPW-ZnO adsorbent: **a** Before adsorption and **b** after adsorption

PPW-ZnO after the adsorption process, showing the existence of contaminants on the surface and the partial filling of craters. Conversely, EDX analysis was used to evaluate the pre- and post-adsorption chemical composition of PPW-ZnO. The EDX profile and elemental mapping analysis found that carbon, oxygen, and zinc are the main components of PPW-ZnO, and the distribution of pore sizes on the PPW-ZnO surface verified the presence of mesopores in the bio composite (as illustrated in Fig. S2).

FT-IR spectra analysis of PPW-ZnO

Fig. 3 shows the FTIR spectrum of PPW-ZnO before and after adsorption, using the PerkinElmer spectrum. O–H stretching vibrations on the adsorbent surface

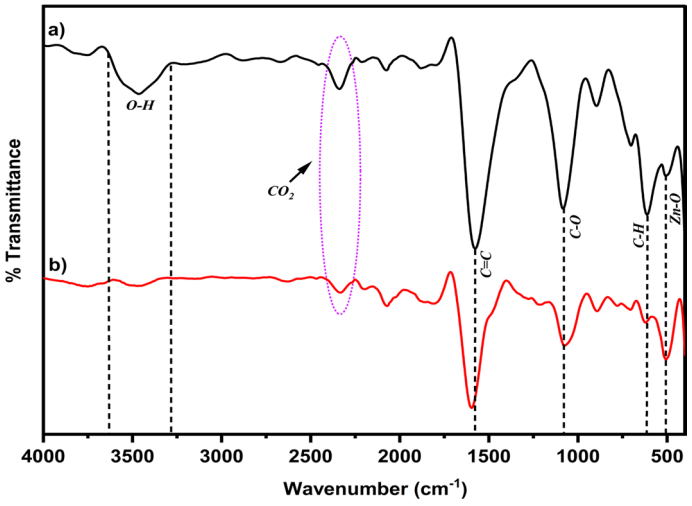

Fig. 3 FTIR spectra: **a** Before and **b** After RhB adsorption on PPW-ZnO

were responsible for the wide band formed by the intermolecular hydrogen banding between 3286 and 3635 cm^{-1} [46], as shown in Fig. 3a where the infrared spectra showed variations in the strengths of adsorption peaks, corresponding to the existence of many functional groups. The detection of carbon dioxide (CO_2) in the air is indicated by a small peak at 2335 cm^{-1}[46]. The significant peak observed at 1576 cm^{-1} indicates C=C stretching vibrations or carboxylic bonds [47]. Polysaccharides, such as cellulose and hemicelluloses, demonstrate an asymmetric stretching vibration of the C–O bond, which can be attributed to a band at 1072 cm^{-1}[48]. Moreover, a peak at 611 cm^{-1} suggests the occurrence of vibrations associated with the C–H bond [49], whereas the narrowing of the peak shows the emergence of Zn–O at 505 cm^{-1}[50].

Fig. 3b illustrates a reduction in peak intensity following the adsorption of RhB, indicating evidence of adsorption on the PPW-ZnO surface, decreased the O–H banding indicate the existence of hydrogen bonding between the PPW-ZnO and RhB molecules. Additionally, the presence of new minor peaks at 1212 cm^{-1} and 780 cm^{-1} provides further evidence of the distinct vibrational patterns exhibited by dye molecules attached to the loaded PPW-ZnO surface [51], as well as the shift of the peak from 1576 cm^{-1} to 1596 cm^{-1}, which might be ascribed to the π–π interaction.

X – ray diffraction analysis (XRD) of PPW-ZnO

XRD analysis is shown in Fig. 4 to illustrate the crystalline properties of the PPW-ZnO bio composite, both before and after adsorption, using the D8 Advance Bruker instrument. The occurrence of a prominent peak at specific angles (2θ values of 31.58°, 34.34°, 36.12°, 47.44°, 56.30°, 62.70°, 67.78°) can be attributed to the ZnO JCPDS (00-036-1451). In an aqueous environment with a neutral pH, an activating agent forms Zn $(OH)_2$ species. This reaction takes place at a temperature of 600 °C and ultimately creates a heterojunction between ZnO and activated carbon, as

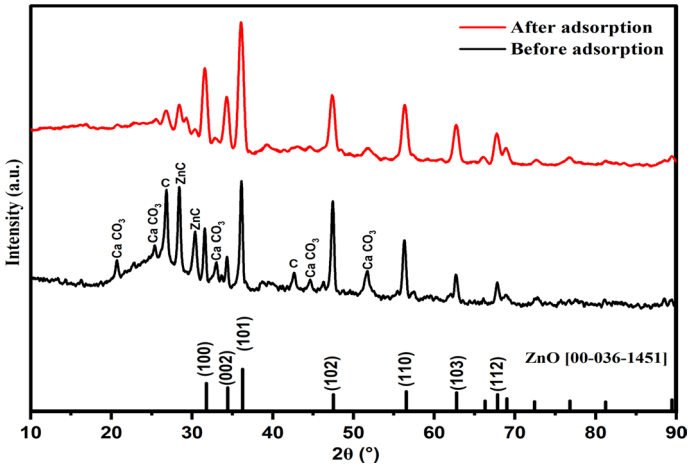

Fig. 4 XRD patterns of PPW-ZnO before and after adsorption

indicated by the findings of previous researchers [52, 53]. Additionally, a series of successive peaks of calcium carbonate ($CaCO_3$) were detected at specific angles 2θ of 20.65°, 25.38°, 33.01°, 44.68°, and 51.78°, as documented in the JCPDS (01-071-2392) database. Conversely, Graphite exhibited peaks at 2θ angles of 26.86° and 42.65° [54], as recorded in the ICDD (00-041-1487) database. Furthermore, zinc carbide was indicated at 2θ angles of 28.39° and 30.38°, as reported in the COD (96-411-9774) database [55]. Nevertheless, the characteristic peaks exhibited a decrease in intensity after the adsorption process. The results confirm the successful adsorption of RhB onto PPW-ZnO adsorbent. In contrast, it is seen that the peaks of zinc oxide persist during the process of adsorption, suggesting the presence of a heterojunction between zinc oxide and activated carbon. Weak bonds are generated between carbon and zinc, rendering them unstable in an aqueous medium.

The optimization of process parameters for the elimination of RhB

The impact of contact duration and the kinetics adsorption

Fig. 5 illustrates the temporal variation in the adsorption of RhB onto PPW-ZnO. The RhB adsorption capacity of PPW-ZnO exhibited a rapid increase, reaching 11.76 mg/g within 10 min, followed by a gradual approach towards equilibrium over 180 min. This is due to the many adsorption sites which are capable

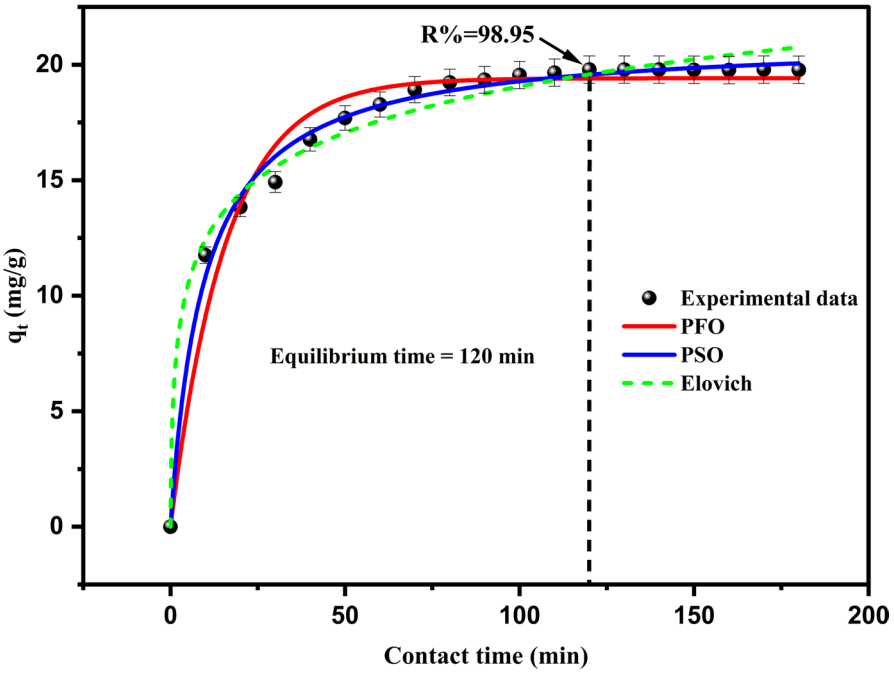

Fig. 5 Kinetics of RhB adsorption ($C_0 = 20$ mg/L, $\frac{m}{V} = 1$ g/L, $T = 20 \pm 1$ °C and neutral pH)

of received the RhB. The intensity of the competition increased as additional sites became occupied by pollutants, leading to a reduced rate of adsorption during the later stage. The equilibrium state of adsorption, was achieved after 120 min, resulting in an adsorption capacity of 19.79 mg/g and a removal efficiency of 98.95%. The presence of surface craters, abundant mesopores, contributes to excellent adhesion of pollutants to the surface of activated carbon [56]. The analysis revealed that the pseudo-second order model exhibit the highest degree of conformity with the experimental data, as evidenced by their superior value of R^2 and small value of χ^2 [57], the results are shown in Table 2.

The experimental results show three different steps in the adsorption process (Fig. S3). The initial phase entails the transfer of the RhB molecule from the outer surface of the adsorbent to the pores within its internal framework. The second stage is the transfer of the RhB molecule from the adsorbent's exterior surface to the pores inside its internal structure, also called intraparticle diffusion [58].

Table 2 Parameter values obtained by modelling the kinetic data

Model	Parameter	Unit	Value/standard error
PFO	q_e	mg/g	19.41 ± 0.24
	K_1	L/min	0.063 ± 0.005
	R^2	–	0.967
	χ^2	–	2.16
PSO	q_e	mg/g	21.12 ± 0.19
	K_2	g/mg min	$0.005 \pm 3 \times 10^{-4}$
	R^2	–	0.992
	χ^2	–	0.50
Elovich	α	mg/g min	20.91 ± 7.6
	β	g/ mg	0.345 ± 0.02
	R^2	–	0.983
	χ^2	–	1.09
Intraparticle diffusion			
First step	K_{IP1}	(mg/g.min$^{0.5}$)	1.46 ± 0.07
	C_1	(mg/g)	7.19 ± 0.41
	R_1^2	–	0.99
	χ^2	–	0.28
Second step	K_{IP2}	(mg/g.min$^{0.5}$)	0.34 ± 0.03
	C_2	(mg/g)	16.12 ± 0.3
	R_2^2	–	0.97
	χ^2	–	0.008
Third step	K_{IP3}	(mg/g.min$^{0.5}$)	0.004 ± 0.003
	C_3	(mg/g)	19.83 ± 0.04
	R_3^2	–	0.24
	χ^2	–	2.7×10^{-4}

Ultimately, the third phase centers on the specific process of adsorption, wherein the RhB molecule adheres to the inside surface of the adsorbent material [59]. Based on the experimental findings, it can be observed that the line representing the third stage demonstrates a notably reduced slope. This phenomenon may be attributable to the drop on the limited availability of active sites. As the researchers found, the observations above indicate that the adsorption process is nearing a state of equilibrium [60].

The impact of ion strength

When the concentration of Na^+ was increased from 0.1 to 1 M, the adsorption capacity of PPW-ZnO for RhB did not change significantly (Fig. S4). Instead, there was a slight drop in adsorption capacity between 19.79 and 19.70 mg/g, indicating that Na^+ had very little effect on RhB adsorption. This discrepancy arises because sodium ions Na^+ and RhB molecules exhibit dissimilar adsorption sites, precluding any form of competitive adsorption. The PPW-ZnO composite demonstrated excellent adsorption properties when subjected to diverse contaminants in complex wastewater compositions, including interfering ions [61].

The impact of pH on solution properties

In the pH range of 2–12, PPW-ZnO shows good RhB adsorption capacity (Fig. 6). This specific phenomenon exemplifies the notion that the inclusion of PPW-ZnO in a particular setting can significantly augment its effectiveness as an adsorbent, particularly in the realm of dye elimination from wastewater in circumstances characterized by severe levels of acidity or alkalinity.

The adsorption capacity of PPW-ZnO for RhB between from 19.78 mg/g to 19.7 mg/g due to elevating the solution pH from 2 to 12. The impact of pH solution on the adsorption efficacy of PPW-ZnO on RhB was shown to be statistically insignificant [56–62], suggesting that electrostatic interaction is unlikely to be the primary determinant of the adsorption mechanism, and indicate may be the presence of pore filling mechanism [63].

The pH-dependent zero charge point (pH_{PZC}) of PPW-ZnO was determined in an aqueous solution containing NaCl at a concentration of 0.01 M. In this experimental procedure, 1 g per liter of PPW-ZnO was introduced into a 100 ml solution of NaCl. The pH of the solution was varied between 2 and 12, and the suspension was stirred for 24 h to allow for incubation. According to the findings from the experiments, PPW-ZnO demonstrated a pH point of zero charge (pH_{PZC}) at a value of 6.8. This suggests that the surface of PPW-ZnO exhibits a positive charge when the pH is below 6.8 and a negative charge when the pH is above the point of zero charge (PZC) [64].

Adsorption isotherm and initial concentration

The adsorption of RhB dye onto PPW-ZnO was investigated in this work at a fixed solid/liquid ratio (1 g/L) and multiple starting dye concentrations (ranging from 5 to 200 mg/L, Fig. S5).

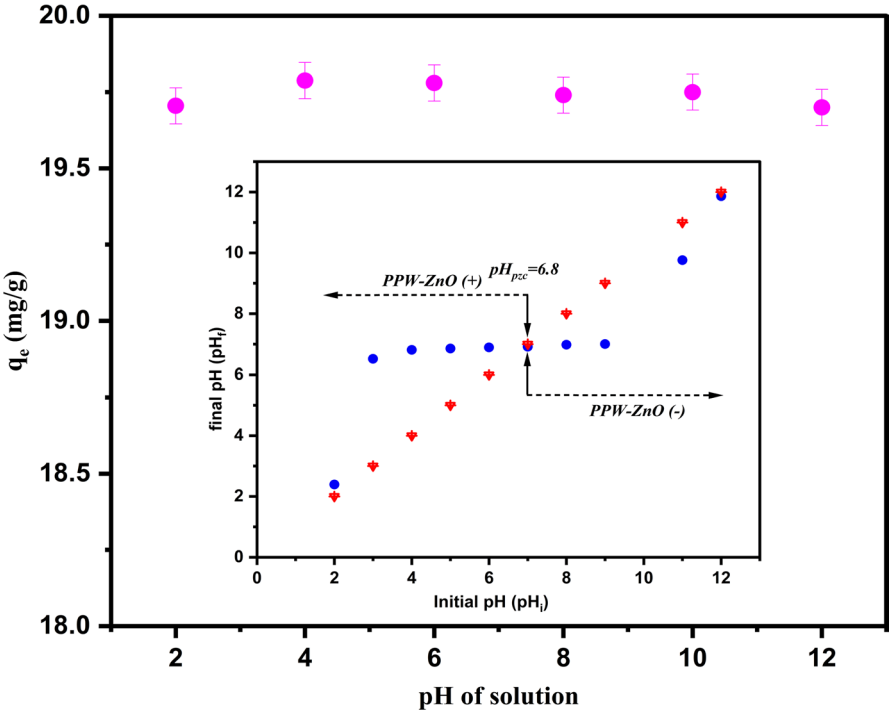

Fig. 6 Effect of pH solution on the RhB adsorption (C_o = 20 mg/L, T = 20 ± 1 °C, t = 120 min, $\frac{m}{V}$ = 1 g/L and initial pH 2–12)

This model also offers insights into the equilibrium behavior, including the capacity and mechanism of the adsorption process (Fig. 7). In addition, the three chosen models explained the data on adsorption equilibrium. The results suggest that the Freundlich model exhibit more suitability in characterizing the adsorption isotherm (the higher value of R^2) and the adsorption process occurred on multiple layers [57], as evidenced by the data presented in the Table 3.

Thermodynamic study

The temperature factor is one of the factors that gives another insight and a clearer understanding of the adsorption process of PPW-ZnO on RhB solution. A solution of rhodamine at concentration 20 mg/L, was studied at three different levels of temperature (298 K, 303 K, and 323 K). The study showed that as the temperature increases, we obtained a decrease in the adsorption capacity of RhB on the PPW-ZnO surface (Fig. S6), and this can be explained, as stated in scientific research, that the binding forces between PPW-ZnO and the RhB may be susceptible to disruption [65].

This process entails the determination of several parameters to obtain a thermodynamic study, including (ΔG°), (ΔH°), (ΔS°) represent the Gibbs free energy change,

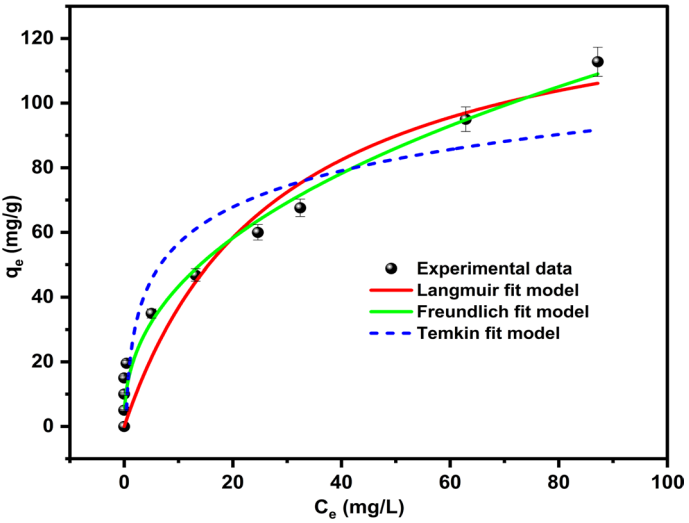

Fig. 7 Isotherms of RhB on PPW-ZnO adsorption (C_o = 5–200 mg/L, T = 20 ± 1 °C, t = 120 min, $\frac{m}{V}$ = 1 g/L and neutral pH)

Table 3 Parameter values obtained by modelling the isotherm data

Model	Unit	Value/standard error
Langmuir		
Q^0_{max}	mg/g	140.34 ± 22.45
K_L	L/mg	0.035 ± 0.014
R^2	–	0.93
χ^2	–	109.22
Freundlich		
n	–	2.38 ± 0.035
K_F	$(mg/g)/(mg/L)^{1/n}$	16.26 ± 2.2
R^2	–	0.98
χ^2	–	24.49
Temkin		
B	–	16.20 ± 2.9
K_g	L/mg	3.29 ± 2.5
R^2	–	0.88
χ^2	–	175.23

enthalpy change and entropy change [66]. These meters can be calculated using the formulae presented in:

$$\Delta G^{\circ} = -RTlnK_e^{\circ} \tag{13}$$

$$lnK_d^{\circ} = -\frac{\Delta H^{\circ}}{RT} + \frac{\Delta S^{\circ}}{R} \quad (14)$$

R expressed in J/mol K the ideal gas constant, temperature T in kelvin (K) and K_d° the thermodynamic equilibrium constant.

The values of several thermodynamic parameters are presented in Table 4. The recorded negative enthalpy (ΔH°) values for the adsorption of Rh B onto PPW-ZnO suggest that the sorption mechanism has an exothermic nature [67]. The presence of negative values Less than 0 for the standard Gibbs energy (ΔG°) suggests that the adsorption reaction is of a spontaneous [68]. Additionally, the negative values of the standard entropy change (ΔS°) indicate a reduction in disorder, this leads to a more orderly arrangement of dye molecules on the adsorption sites.

The process of regenerating PPW-ZnO

In the first cycle as shown in Fig. 8, the PPW-ZnO exhibits a significant abundance of active sites readily available for adsorption. Simultaneously, the activated carbon's pores remain unoccupied, facilitating the dye's adsorption. In the second and third cycles of the PPW-ZnO system, it is observed that certain active sites become occupied by RhB molecules. The decrease in efficacy can be attributed to the partial obstruction of the pores and potential alterations in the surface chemistry of the charcoal. Interestingly, an increase in adsorption capacity was seen during the fourth cycle of the regeneration process. This phenomenon is atypical and implies a modification in the properties of the activated carbon. Several potential explanations could be considered: The elimination of previously adsorbed chemicals that obstruct active sites may be attributed to alterations in the regeneration process [69]. Modifying the activated carbon's structure can enhance the accessibility of active sites or generate novel adsorption sites alterations in the activated carbon surface's chemical composition to an enhanced attraction towards the RhB dye. Table 5 compares our investigation with the published literature, and it is evident that the PPW-ZnO considered competitive with various adsorbents in its efficiency on adsorption of RhB.

Conclusion

A novel bio-composite PPW-ZnO adsorbent, which is prepared by immersing in $ZnCl_2$ solution, that showed forms of ZnO, it also changed the surface area and shape of the exterior of the bio composite to prepare for effective adsorption between PPW-ZnO and RhB. The results showed a high adsorption capacity RhB and a strong attraction

Table 4 Thermodynamics parameters of PPW-ZnO

Bio composite	ΔG° (kJ/mol)			ΔH° (kJ/mol)	ΔS° (kJ/mol K)
	293 K	303 K	323 K		
PPW-ZnO	− 0.54	− 0.48	− 0.094	− 6.011 ± 0.38	− 0.018 ± 0.001

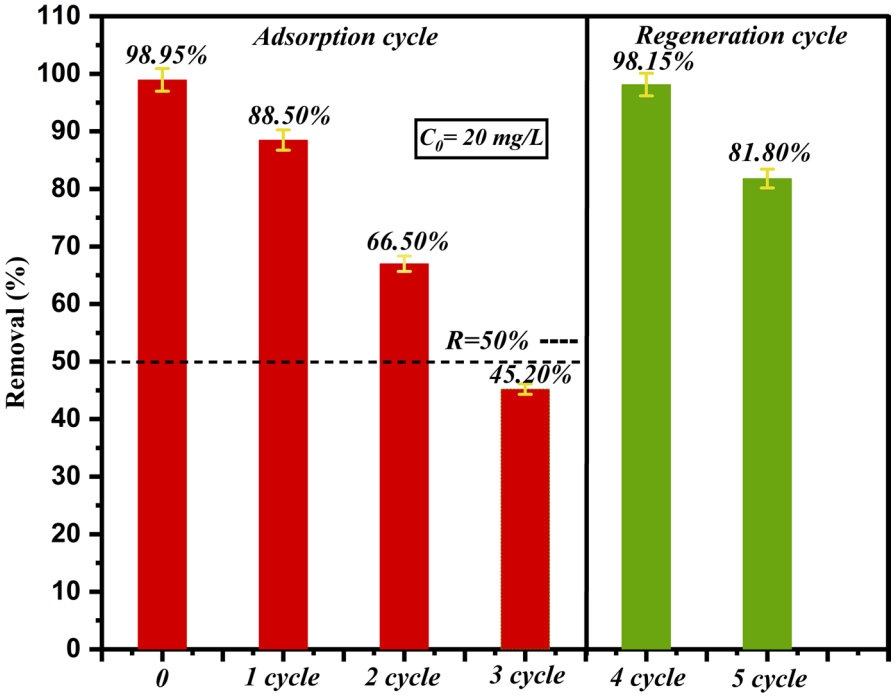

Fig. 8 Adsorption cycles of PPW-ZnO and the regeneration cycle of the bio composite (C_o = 20 mg/L, T = 20 ± 1 °C, t = 120 min, = $\frac{m}{V}$1 g/L and neutral pH)

Table 5 The adsorption efficiency of RhB on various literature studies

Adsorbent	%Removal	References
PPW-ZnO	98.95	This work
Oil-based drill cutting ash (M3-OBDCA)	81.3	[70]
Cassava slag biochar	96	[71]
Kaolinite	95	[72]
Biochar derived from tapioca peel	81.8	[73]
Chamaecyparis lawsoniana fruit	85.42	[74]

between PPW-ZnO and RhB. As well as the hydrogen banding, π-π interaction and pore filling mechanism play an important role in the adsorption process. This is remarkable that it is not affected by the change of the pH RhB solution to the solution and the presence of other ions like Na^+, which makes it a strong competitor to other types of adsorbents. The adsorption capability of RhB exhibits a decrease as the temperature increases. The pseudo-second order kinetic model and the Freundlich isotherm can best describe the adsorption process of the RhB.

Supplementary Information The online version contains supplementary material available at https://doi.org/10.1007/s11144-024-02567-4.

Acknowledgements We thank Pr. Mohamed Toufik Soltani, of Photonic physics and multifunctional nanomaterials- university of Biskra (Algeria), and CRAPC Biskra and Laghouat (Algeria) for its cooperation in characterization measurements. We would also like to thank Naili Radia, and Ben Machiche Hayet (Laboratory of industrial chemistry and laboratory of chemistry- university of biskra, Algeria) for his invaluable assistance in the laboratory.

References

1. Naseem T, Durrani T (2021) The role of some important metal oxide nanoparticles for wastewater and antibacterial applications: a review. J Environ Chem Ecotoxicol 3:59–75
2. Tanji K, El Mrabet I, Fahoul Y, Soussi A, Belghiti M, Jellal I, Naciri Y, El Gaidoumi A, Kherbeche A (2023) Experimental and theoretical investigation of enhancing the photocatalytic activity of Mg doped ZnO for nitrophenol degradation. React Kinet Mech Catal 136:1125–1142
3. Ma R, Nie D, Sang M, Wang W, Nie G (2023) Adsorption of rhodamine B and Pb (II) from aqueous solution by MoS_2nanosheet modified biochar: fabrication, performance, and mechanisms. Bioresour Technol 386:129548
4. Pompeu LD, Muraro PCL, Chuy G, Vizzotto BS, Pavoski G, Espinosa DCR, Fernandes LDS, William LdS (2022) Adsorption for rhodamine B dye and biological activity of nano-porous chitosan from shrimp shells. Environ Sci Pollut Res 29(33):49858–49869
5. Benammar S, Haffas M, Hamitouche A, Boudjemaa A, Bachari K (2022) Relevance of *Anethum graveolens* to remove rhodamine B in aqueous solution: characterization, kinetic and isotherm study. React Kinet Mech Catal 136(1):465–490
6. Sh GM, Abd-Elhamid AI, El-Shanshory AA, Soliman HMA (2022) Adsorption of cationic dyes onto chemically modified activated carbon: kinetics and thermodynamic study. J Mol Liq 346:118227
7. Zbair M, Anfar Z, Ait Ahsaine H, El Alem N, Ezahri M (2018) Acridine orange adsorption by zinc oxide/almond shell activated carbon composite: operational factors, mechanism, and performance optimization using central composite design and surface modeling. J Environ Manage 206:383–397
8. Belghiti M, Tanji K, El Mersly L, Lamsayety I, Ouzaouit K, Faqir H, Benzakour I, Rafqah S, Outzourhit A (2022) Fast and non-selective photodegradation of basic yellow 28, malachite green, tetracycline, and sulfamethazine using a nanosized ZnO synthesized from zinc ore. React Kinet Mech Catal 135:2265–2278
9. Daouda A, Honorine AT, Bertrand NG, Richard D, Domga. (2019) Adsorption of rhodamine B onto orange peel powder. Am J Chem 9(5):142–149
10. Jia M, Liu C, Cui X, Yu S, Chen K (2023) Fast and efficient adsorption of the organic dyes on the porous carbon microspheres prepared from a new two-step approach. Diam Relat Mater 131:109604
11. Pompeu LD, Druzian DM, Oviedo LR, Viana AR, Mortari SR, Pavoski G, Espinosa DCR, Vizzotto BS, Fernandes LS, da Silva WL (2023) Adsorption of rhodamine B dye onto novel biochar: isotherm, kinetic, thermodynamic study, and antibiofilm activity. Inorg Chem Commun 158:111509
12. Zhao C, Wang B, Theng BKG, Wu P, Liu F, Wang S, Lee X, Chen M, Li L, Zhang X (2021) Formation and mechanisms of nano-metal oxide-biochar composites for pollutants removal: a review. Sci Total Environ 767:145305
13. Bala K, Sharma D, Kumar N, Gupta N, Raja V (2023) Tea waste–derived charcoal as an efficient adsorbent for the removal of rhodamine B. Biomass Convers Bi. https://doi.org/10.1007/s13399-023-04823-4
14. Da Rosaa ALD, Carissimia E, Dotto GL, Sanderc H, Feris LA (2018) Biosorption of rhodamine B dye from dyeing stones effluents using the green microalgae *Chlorella pyrenoidosa*. J Clean Prod 198:1302–1310
15. Chennah A, Ali Khan M, Zbair M, Ait AH (2023) NiO/AC active electrode for the electrosorption of rhodamine B: structural characterizations and kinetic study. Catalysts 13(6):1009
16. Naboulsi A, Naboulsi I, Regti A, El Himri M, El Haddad M (2023) The valorization of rosemary waste as a new biosorbent to eliminate the rhodamine B dye. Microchem J 191:108790
17. Mbarki F, Selmi T, Kesraoui A, Seffen M (2022) Low-cost activated carbon preparation from corn stigmata fibers chemically activated using H_3PO_4, $ZnCl_2$, and KOH: study of methylene blue adsorption, stochastic isotherm, and fractal kinetic. Ind Crops Prod 178:114546

18. Kiełbasa K, Bayar S, Varol EA, nscek-Nazzal J, Bosacka M, Miadlicki P, Serafin J, J. Wróbel R, Michalkiewicz B. (2022) Carbon dioxide adsorption over activated carbons produced from molasses using H_2SO_4, H_3PO_4, HCl, NaOH, and KOH as activating agents. Molecules 27:7467
19. Li R, Wang Z, Guo J, Li Y, Zhang H, Zhu J, Xie X (2018) Enhanced adsorption of ciprofloxacin by KOH modified biochar derived from potato stems and leaves. Water Sci Technol 77(3–4):1127–1136
20. Guo N, Lv X, Yang Qi XuX, Song H (2021) Effective removal of hexavalent chromium from aqueous solution by $ZnCl_2$ modified biochar: Effects and response sequence of the functional groups. J Mol Liq 334:116149
21. Alshandoudi LM, Alkindi SR, Alhatmi TY, Hassan AF (2023) Synthesis and characterization of nano zinc oxide/zinc chloride–activated carbon composite based on date palm fronds: adsorption of methylene blue. Biomass Convers Biorefin. https://doi.org/10.1007/s13399-023-03815-8
22. Faizal ANM, Meskam NN, Putra NR, Zaini AS, Rusli NM, Zaini MAA (2023) Preparation of beeswax residue-$ZnCl_2$-activated carbon for adsorption of methylene blue. Mater Today Proc. https://doi.org/10.1016/j.matpr.2023.08.345
23. Zhang G, Yang H, Jiang M, Zhang Q (2022) Preparation and characterization of activated carbon derived from deashing coal slime with $ZnCl_2$ activation. Colloids Surf A Physicochem Eng Asp 641:128124
24. Li F, Zimmerman AR, Hu X, Yu Z, Huang J, Gao B (2020) One-pot synthesis and characterization of engineered hydrochar by hydrothermal carbonization of biomass with $ZnCl_2$. Chemosphere 254:126866
25. Zhao H, Zhong H, Jiang Y, Li H, Tang P, Li D, Feng Y (2022) Porous $ZnCl_2$-activated carbon from shaddock peel: methylene blue adsorption behavior. Materials (Basel) 15:895
26. Li Y, Liu X (2014) Activated carbon/ZnO composites prepared using hydrochars as an intermediate and their electrochemical performance in supercapacitor. Mater Chem Phys 148(1–2):380–386
27. Djebri A, Belmedani M, Belhamdi B, Trari M, Sadaoui Z (2021) The combined effectiveness of activated carbon (AC)/ZnO for the adsorption of mebeverine hydrochloride/photocatalytic degradation under sunlight. React Kinet Mech Catal 132:529–546
28. Kadam P, Gadave KM, Jadkar S, Kadam V, Jagtap C (2023) C: ZnO Composites for improving catalytic activity of ZnO. ES Energy Environ 2023(21):946
29. Zghal S, Jedidi I, Cretin M, Cerneaux S, Abdelmouleh M (2023) Adsorptive removal of rhodamine B dye using carbon graphite/cnt composites as adsorbents: kinetics. Isotherms Thermodyn Study Mater 16:1015
30. Hoang LP, Van HT, Nguyen TTH, Nguyen VQ, Quang TP (2020) Coconut shell activated carbon/$CoFe_2O_4$ composite for the removal of rhodamine B from aqueous solution. J Chem 2020:1–12
31. Song Y, Wang K, Zhao F, Du Z, Zhong B, An G (2022) Preparation of powdered activated carbon composite material and its adsorption performance and mechanisms for removing RhB. Water 14:3048
32. Akl MA, Mostafa AG, Al-Awadhi M, Al-Harwi WS, El-Zeny AS (2023) Zinc chloride activated carbon derived from date pits for efficient biosorption of brilliant green: adsorption characteristics and mechanism study. Appl Water Sci 13(12):226
33. Ye T, Liu L, Wang Y, Zhang J, Wang Z, Li C, Luo H (2023) Efficient degradation of rhodamine B dye through hand warmer heterogeneous activation of persulfate. Sustainability 15(17):13034
34. Hadj-Otmane C, Ouakouak A, Touahra F, Grabi H, Martín J, Bilal M (2022) Date palm petiole–derived biochar: effect of pyrolysis temperature and adsorption properties of hazardous cationic dye from water. Biomass Convers Biorefin. https://doi.org/10.1007/s13399-022-03127-3
35. Xiao W, Garba ZN, Sun Z, Lawan I, Wang L, Lin M, Yuan Z (2020) Preparation and evaluation of an effective activated carbon from white sugar for the adsorption of rhodamine B dye. J Clean Prod 253:119989
36. Lima DR, Bandegharaei AH, Thue PS, Lima EC, de Albuquerque YRT, dos Reis GS, Umpierres CS, Dias SLP, Tran HN (2019) Efficient acetaminophen removal from water and hospital effluents treatment by activated carbons derived from Brazil nutshells. Colloids Surf a Physicochem Eng Asp 583:123966
37. Jawad AH, Ismail K, Ishak MAM, Wilson LD (2019) Conversion of Malaysian low-rank coal to mesoporous activated carbon: structure characterization and adsorption properties. Chin J Chem 27:1716–1727
38. Ghibate R, Senhaji O, Taouil R (2021) Kinetic and thermodynamic approaches on rhodamine B adsorption onto pomegranate peel. Case Stud Chem Environ Eng 3:100078

39. Inyinbor AA, Adekola FA, Olatunji GA (2016) Kinetics, isotherms and thermodynamic modeling of liquid phase adsorption of rhodamine B dye onto Raphia hookerie fruit epicarp. Water Resour Ind 15:14–27
40. Saufi H, Alouani EL, M, Aride J, Taibi M. (2020) Rhodamine B biosorption from aqueous solution using *Eichhornia crassipes* powders: Isotherm, kinetic and thermodynamic studies. Chem Data Collect 25:100330
41. Pompeu LD, Druzian DM, Oviedo LR, Viana AR, Mortari SR, Pavoski G, Espinosa DCR, Vizzotto BS, Fernandes LS, da Silva WL (2023) Adsorption of rhodamine b dye onto novel biochar: isotherm, kinetic, thermodynamic study and antibiofilm activity. Inorg Chem Commun 158:111509
42. Azizia A, Monirib E, Hassania AH, Panahic HA, Jafarinezhadd M (2021) Nonlinear and linear analysis of direct yellow 50 adsorption onto modified graphene oxide: kinetic, isotherm, and thermodynamic studies. Desalin Water Treat 229:352–361
43. Chebbi M, Ounoki S, Youcefa L, Amrane A (2023) Synthesis and characterization of pine cones biochar for the removal of an antibiotic (Metronidazole) from aqueous solutions. J Ind Eng Chem 126:327–339
44. Thommes M, Kaneko K, Neimark AV, Olivier JP, Reinoso FR, Rouquerol J, Sing KSW (2015) Physisorption of gases, with special reference to the evaluation of surface area and pore size distribution (IUPAC Technical Report). Pure Appl Chem 87(9–10):1051–1069
45. Dos Reis GS, Guy M, Mathieu M, Jebrane M, Lima EC, Thyrel M, Dotto GL, Larsson SH (2022) A comparative study of chemical treatment by $MgCl_2$, $ZnSO_4$, $ZnCl_2$, and KOH on physicochemical properties and acetaminophen adsorption performance of biobased porous materials from tree bark residues. Colloids Surf A Physicochem Eng Asp 642:128626
46. Ni X, Sun X, Xu Y, Xu D (2022) A green and facile synthesis of nosean composite from coal fly ash for optimizing rhodamine B adsorption using response surface methodology. J Mol Liq 359:119262
47. Nazir R, Khan M, Rehman RU, Shujah S, Khan M, Ullah M, Zada A, Mahmood N, Ahmad I (2020) Adsorption of selected azo dyes from an aqueous solution by activated carbon derived from *Monotheca buxifolia* waste seeds. Soil Water Res 15(3):166–172
48. Salem DB, Ouakouak A, Touahra F, Hamdi N, Eltaweil AS, Syed A, Boopathy R, Tran HN (2023) Easy separable, floatable, and recyclable magnetic-biochar/alginate bead as super-adsorbent for adsorbing copper ions in water media. Bioresour Technol 383:129225
49. Rouahna N, Salem DB, Bouchareb I, Nouioua A, Ouakouak A, Fadel A, Hamdi N, Boopathy R (2023) Reduction of crystal violet dye from water by pomegranate peel-derived efficient biochar: influencing factors and adsorption behaviour. Water Air Soil Pollut 234(5):324
50. Da Silva WL, Muraro PCL, Pavoski G, Espinosa DCR, dos Santos JHZ (2022) Preparation and characterization of biochar from cement waste for removal of rhodamine B dye. J Mater Cycles Waste Manag 24(4):1333–1342
51. Suresh G, Kumaresan P, Nihiyanantham S, Kumar KS, Ambalavanan P (2019) Rhodamine-B doped zinc (Tris) thiourea sulphate crystals for NLO applications with DFT approach. Chem Sci Trans 8(1):133–145
52. Rehali H, Menasra H, Djebabra S, Aidi A, Bekiri F, Benbrika C, Hamida K (2023) Structural and morphological properties of (Ns Bc/Zno) bio-composite adsorption. Tob Regul Sci. https://doi.org/10.18001/TRS.9.2.75
53. Li B, Li C, Li D, Zhang L, Zhang S, Cui Z, Wang D, Tang Y, Hu X (2023) Activation of pine needles with zinc chloride: evolution of functionalities and structures of activated carbon versus increasing temperature. Fuel Process Technol 252:107987
54. Hanafi NAM, Abdulhameed AS, Jawad AH, Al Othman ZA, Yousef TA, Alduaij OK, Al Saiari NS (2022) Optimized removal process and tailored adsorption mechanism of crystal violet and methylene blue dyes by activated carbon derived from mixed orange peel and watermelon rind using microwave-induced $ZnCl_2$ activation. Biomass Convers Biorefin. https://doi.org/10.1007/s13399-022-03646-z
55. Tiotsop Kuete IH, Tchuifon RDT, Bopda A, Ngakou CS, Nche GNA, Anagho SG (2022) Adsorption of Indigo carmine onto chemically activated carbons derived from the cameroonian agricultural waste garcinia cola nut shells and desorption studies. J Chem 2022:19
56. Wang Q, He D, Li C, Sun Z, Mu J (2023) Honeycomb-like cork activated carbon modified with carbon dots for high-efficient adsorption of Pb(II) and rhodamine B. Ind Crops Prod 196:116485
57. Dra A, Tanji K, Arrahli A, Iboustaten EM, El Gaidoumi A, Kherchafi A, Benabdallah AC, Kherbeche A (2020) Valorization of Oued Sebou natural sediments (Fez-Morocco Area) as adsorbent of methylene blue dye: kinetic and thermodynamic study. Sci World J. https://doi.org/10.1155/2020/2187129

58. Jabar JM, Adebayo MA, Owokotomo IA, Odusote YA, Yılmaz M (2022) Synthesis of high surface area mesoporous $ZnCl_2$–activated cocoa (*Theobroma cacao* L.) leaves biochar derived via pyrolysis for crystal violet dye removal. Heliyon 8(10):10873
59. Zamouche M, Hamdaoui O (2012) Sorption of rhodamine B by cedar cone: effect of pH and ionic strength. Energy Procedia 18:1228–1239
60. Gong J, Liu R, Sun Y, Xu J, Liang M, Sun Y, Long L (2024) Preparation of high-performance nitrogen-doped porous carbon from cork biomass by K_2CO_3 activation for adsorption of rhodamine B. Ind Crops Prod 208:117846
61. Dabagh A, Benhiti R, Abali M, Ait Ichou A, Sinan F, Zerbet M (2023) Valorization of plant biomass by chemical pretreatment: application to the removal of rhodamine B and congo red dyes. Biomass Convers Biorefin. https://doi.org/10.1007/s13399-023-04299-2
62. Li P, Zhao T, Zhao Z, Tang H, Feng W, Zhang Z (2023) Biochar derived from Chinese herb medicine residues for rhodamine B dye adsorption. ACS Omega 8(5):4813–4825
63. Fan X, Wang X, Cai Y, Xie H, Han S, Hao C (2021) Functionalized cotton charcoal/chitosan biomass-based hydrogel for capturing Pb^{2+}, Cu^{2+} and MB. J Hazard Mater 423:127191
64. Abbas M, Harrache Z (2019) Removal of gentian violet in aqueous solution by activated carbon equilibrium, kinetics, and thermodynamic study. Adsorpt Sci Technol 37(7–8):566–589
65. Li X, Xu J, Luo X, Shi J (2022) Efficient adsorption of dyes from aqueous solution using a novel functionalized magnetic biochar: synthesis, kinetics, isotherms, adsorption mechanism, and reusability. Bioresour Technol 360:127526
66. Ahmed HR, Radha FHS, Agha NNM, Amin KFM, Shwan DMS (2023) Characterization and evaluation of *Moringa oleifera* leaves green powder and its alkali-activated form as eco-friendly biosorbent for the effective removal of safranin dye from synthetic wastewater. React Kinet Mech Catal 136:2181–2201
67. Foroutan R, Peighambardoust SJ, Peighambardoust SH, Pateiro M, Lorenzo JM (2021) Adsorption of crystal violet dye using activated carbon of lemon wood and activated carbon/Fe_3O_4 magnetic nanocomposite from aqueous solutions: a kinetic, equilibrium and thermodynamic study. Molecules 26(8):2241
68. Alswieleh AM (2023) Kinetic, equilibrium and thermodynamic studies for rhodamine B adsorption on sodium tauroglycocholate functionalized mesoporous silica nanoparticles. J Porous Mater 30(3):937–948
69. Nouioua A, Salem DB, Ouakouak A, Rouahna N, Baigenzhenov O, Hosseini-Bandegharaei A (2023) Production of biochar from Melia azedarach seeds for the crystal violet dye removal from water: combining of hydrothermal carbonization and pyrolysis. Bioengineered 14(1):290–306
70. Zhao Y, Yang H, Sun J, Zhang Y, Xia S (2021) Enhanced adsorption of rhodamine b on modified oil-based drill cutting ash: characterization, adsorption kinetics, and adsorption isotherm. ACS Omega 6:17086–17094
71. Wu J, Yang J, Huang G, Xu C, Lin B (2020) Hydrothermal carbonization synthesis of cassava slag biochar with excellent adsorption performance for rhodamine B. J Clean Prod 251:119717
72. El Hassani AA, Tanji K, El Mrabet I, Fahoul Y, El Gaidoumi A, Benjelloun AT, Sfaira M, Zaitan H, Kherbeche A (2023) A combined molecular dynamics simulation, DFT calculations, and experimental study of the adsorption of rhodamine B dye on kaolinite and hydroxyapatite in aqueous solutions. Surf Interfaces 36:102647
73. Vigneshwaran S, Sirajudheen P, Karthikeyan P, Meenakshi S (2021) Fabrication of sulfur-doped biochar derived from tapioca peel waste with superior adsorption performance for the removal of malachite green and rhodamine B dyes. Surf Interfaces 23:100920
74. Gul S, Gul H, Gul M, Khattak R, Rukh G, Khan MS, Aouissi HA (2022) Enhanced adsorption of rhodamine b on biomass of cypress/false cypress (*Chamaecyparis lawsoniana*) fruit: optimization and kinetic study. Water 14:2987